Ablation effects and mechanism of sintered silicon carbide ceramics by an ArF excimer laser

Xin Guo (郭 馨)*, Jinbin Ding (丁金滨), Yi Zhou (周 翊), and Yu Wang (王 宇)

Academy of Opto-Electronics, Chinese Academy of Sciences, Beijing 100094, China
**Corresponding author: gx_06@163.com*

Received February 5, 2018; accepted July 25, 2018; posted online August 31, 2018

The ablation of sintered silicon carbide ceramics by an ArF excimer laser was studied. Three zones are generated: the ablation zone that presented molten morphology and was composed by the Si and C phase; the condensation zone formed by vaporized SiC; and the oxidation zone that showed the characteristics of thermal oxidation. The ablation depth and oxidation range increase linearly with fluence and pulses within 0.5–4 J/cm^2, but the normalized ablation efficiency is constant (3.60 ± 0.60 μm · mm^2/J). The theoretical photochemical ablation depth supplies 25% of the total depth at 1 J/cm^2 but decreases to 16% at 4 J/cm^2. The ablation is dominated by the photothermal effect and conforms to the thermal evaporation mechanism.

OCIS codes: 140.3390, 140.2180, 160.6000.
doi: 10.3788/COL201816.091402.

SiC ceramics have excellent physical, chemical, and electrical properties and are widely used in aerospace, mechanical, electronic, energy, chemical, and other fields[1,2]. However, the high hardness and low fracture toughness make it difficult to process and easy to form contact microcracks, greatly limiting its application[3,4].

With a high output energy and a large single-photon energy, excimer lasers can achieve non-contact microprocessing by photothermal and photochemical effects. They are suitable for hard and brittle materials such as ceramics[5,6]. However, affected by laser parameters, material properties, and environmental factors, the interactions between the laser and the material are complicated[7,8]. Research has found that laser wavelength and pulse width seriously affect the ablation process[9,10]. Lasers with short wavelengths have a high single-photon energy to realize the photochemical reaction, but the nanosecond pulse width makes the ablation contain heating and melting on the nanosecond scale and subsequent rapid solidification cooling[11]. As a result, the ablation effects of different materials may differ. Sciti, Hua, and Xie *et al.* found that ablation of Al_2O_3 by the excimer laser was dominated by the photothermal mechanism, since Al_2O_3 mainly decomposed and evaporated[12–14]. Li thought that the ablation of single-crystal silicon was dominated by the photothermal mechanism, but the ablation of glass and diamond film by the excimer laser was dominated by the photochemical mechanism[15].

For SiC materials, their bandgap energy (about 3.00 eV) is lower than the single-photon energy of the 193 nm excimer laser (6.44 eV), the single-photon energy can interrupt the Si-C bond, and the photochemical reaction could occur. But the nanosecond pulse width also suggests the thermal effect. The ablation threshold (F_{th}) and influence factors of SiC materials were tested and modeling was analyzed[16,17]. It was found that the phases affect the ablation behavior and F_{th}, $F_{\mathrm{th(c\text{-}SiC)}}$ was over twice that of $F_{\mathrm{th(\alpha\text{-}SiC)}}$. Therefore, the ablation effect could strongly depend on the laser parameters, the initial state of SiC, and the environment. Sciti *et al.* found the ablation of SiC was dominated by the photothermal mechanism, with melting morphology detected under a high laser fluence (7.5 J/cm^2, higher than the F_{th} of 0.26–0.8 J/cm^2) and the SiC was oxidized[12]. But Zhang had found that the Si phase was retained under a low laser fluence[18]. To understand the ablation of SiC, the material initial state, the material behavior, the phase variation, and the influence of the laser parameters and environmental factors need systemic and quantitative study.

In this Letter, since the 193 nm ArF excimer laser meets the highest absorption coefficient wavelength (70 nm to 200 nm), and the pulse reduces the heat affected zone, the ArF laser is selected in the experiment. To avoid the thermal turbulence caused by the protective gas and reduce the interaction between the SiC and the air, a small spot under the air conditioner was selected to retain the reaction form of the ablated sintered silicon carbide ceramics (S-SiC ceramics) by the ArF excimer laser. Under the premise of reducing the environmental impact, the study can be done quantitatively. The morphology, composition, and phase distribution were characterized, the ablation behaviors were revealed, the influence of the laser parameters on the ablation effect and efficiency was analyzed, and the ablation mechanism of the SiC ceramics by the excimer laser was discussed. It will provide theoretical guidance and an experimental basis for the ablation-based laser process for SiC ceramics.

The irradiation source was an independently developed ArF excimer laser with a wavelength of 193 nm, a designed repetition rate of 10 Hz–4 kHz, a maximum power of 40 W at 4 kHz, and a pulse width of 20 ns. The laser beam passed through the CaF_2 reflector and the focusing lens, and then came to the ceramic fixed on the 3-axis translation platform. A positive defocus of about 0.1 mm was used to

avoid the evaporation holes caused by the exorbitant fluence. A small spot size (250 μm × 50 μm) and the air conditioner were used to minimize the environmental impact. The change of the output power of the laser and an appropriately fine adjustment of the defocus were used to achieve the spot size and laser fluence requirements.

Non-pressed sintered S-SiC ceramics (Kema Tek) were used in the experiment, whose thermal conductivity was 120 $W/(m \cdot K)$ and specific heat was $0.65 \times 10^3 J/(kg \cdot K)$. The ceramics were mechanically polished to Ra = 0.5 μm and ultrasonically cleaned before the ablation experiment. The morphology of SiC ceramics was observed with an optical microscope (Olympus, BX51) and a scanning electron microscope (SEM, JEOL, JSM-7001 F). The composition was detected by energy dispersive spectroscopy after streaming a conductive Pt film. Map scanning was used to reduce the error caused by the unevenness distribution of the elements. The phase of the ablation and affected zones was measured with a Raman analyzer (Horiba Jobin Yvon, LabRAM HR-800), and the analyzer was calibrated by the characteristic peak of SiC in the raw area. The excitation laser used was an Ar ion laser with a wavelength of 514.5 nm. The roughness and ablation depth were characterized by the 3D surface profilometer (Zygo, NewView8300).

When the laser fluence exceeded the ablation threshold of SiC, the morphology and phase of the ablated SiC ceramics would change. Figure 1 shows the optical morphology and the typical 3D profile of the ablated SiC. The material of the ablation zone melts and the surrounding presents a color change gradually from orange, to blue, to brown. Obviously, the surrounding zone is oxidized in the atmospheric condition, and the color variation is normally caused by the difference in oxidation degree and the oxidation depth. According to the studies on silicon oxide[19], the typical thicknesses of the orange, blue, brown, and silvery films are 0.24, 0.12, 0.05, and 0.02 μm. The thickness distribution of the colored zone conforms to the distribution rule of thermal oxide layers.

At the edge of the ablation zone, spattering is distributed. The laser ablated material rapidly vaporizes out of the ablation zone under the high temperature and pressure, rapidly condenses, and forms the spattering structure. The height of the spatter is reduced at low laser fluence, so the condensation zone can be controlled by restricting the fluence. Through the above analysis, the SiC ceramics ablated by the excimer laser can be divided into the ablation zone, the condensation zone, and the oxidation zone.

Figure 2 is the SEM morphology of the matrix and the ablation zone. The matrix shows a typical mechanically polished morphology, containing scratches and pores. But after being ablated by the excimer laser, the mechanical damage defects have been effectively eliminated and the ceramics show a molten state with a small amount of vaporized pores and cooling droplet form. No obvious oxidation is detected in the ablation zone.

To further clarify the influence of the ablation, the composition distribution of the ablation and affected zone was detected, as shown in Figs. 3(a) and 3(b). The decomposition reaction of SiC ceramics can occur in the case of discontinuous melting, so a large number of Si and C phases will melt and evaporate, and consume the oxygen near the surface. The low energy ensures quick condensation, and the low oxygen content limits the oxidation rate, so the ablation zone is not obviously oxidized. However, the energy of the beam heats the surrounding materials and makes them tend to be oxidized. Small oxide particles with an oxygen mass percentage over 25% can be observed beside the condensation zone. A single pulse irritated on the left of the ablation zone does not induce any morphology variation but eliminates the oxygenation layer caused by the thermal effect. So, the depth of the oxidation layer is lower than the ablation depth of a single pulse under the experimental parameters.

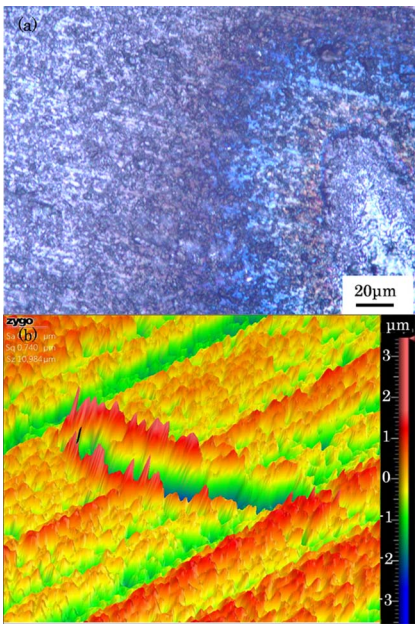

Fig. 1. Morphology of ablated SiC ceramics at 3.1 J/cm^2, 50 pulses: (a) the optical morphology; (b) the 3D profile.

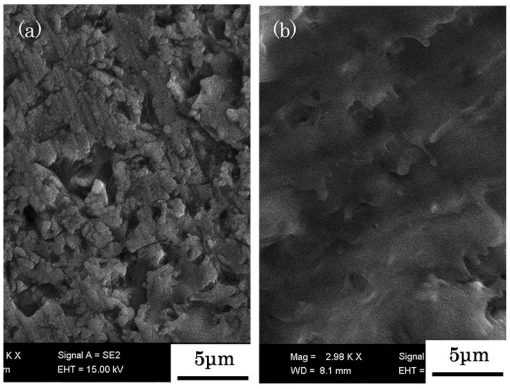

Fig. 2. (a) Morphology of the matrix and (b) the ablation zone at 3.1 J/cm^2, 50 pulses.

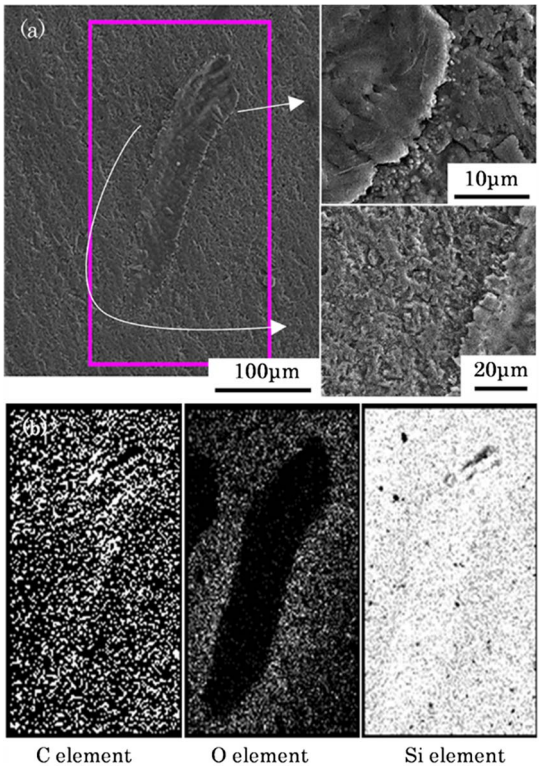

Fig. 3. (a) Morphology and (b) composition of the ablated SiC ceramics at 3.1 J/cm^2, 50 pulses.

The composition of the SiC ceramics was tested. The $\omega(\mathrm{C{:}Si})_{\mathrm{matrix}}$ is 42.8:57.2, and the $\omega(\mathrm{C{:}O{:}Si})_{\mathrm{ablation}}$ is 39.99:1.39:58.63. The composition of the ablation zone is basically similar to that of the matrix, except for a slight oxidation. The $\omega(\mathrm{C{:}O{:}Si})_{\mathrm{oxidation}}$ close to the condensation zone is 29.05:20.32:50.64, while the ω(C:O:Si) 30 μm away is 30.12:15.68:54.2. The CO or CO_2 gaseous products decrease the C content, but the penetration/combination of oxygen increases the O content.

Figure 4 shows the phases of the ablation zone, condensation zone, oxidation zone, and the matrix of the SiC tested by the Raman spectrum. The peaks at 147, 766, 788, and 969 cm^{-1} are the characteristic peaks of α-SiC and β-SiC. The peaks at 1360 cm^{-1} and 1580 cm^{-1} are the disordered structure D line of amorphous carbon and the characteristic G line of the graphite. Near 450–550 cm^{-1} an obvious wide peak appears, which corresponds to the characteristic peak of the Si phase. So the matrix of the S-SiC ceramics is composed by the SiC phase and graphite phase or amorphous carbon. The ablation zone is mainly composed of the Si phase and graphite phase or amorphous carbon, in which the Si phase contains the α-Si and c-Si phase. The width of the D line increases and overlaps with the G line, indicating that the disorder degree of the C element rises. It also contains some of the α-SiC phase, which should be recombined from the decomposed Si and C in the cooling stage, or the matrix phase detected by the penetrating polishing layer. The phases of the condensation and oxidation zones

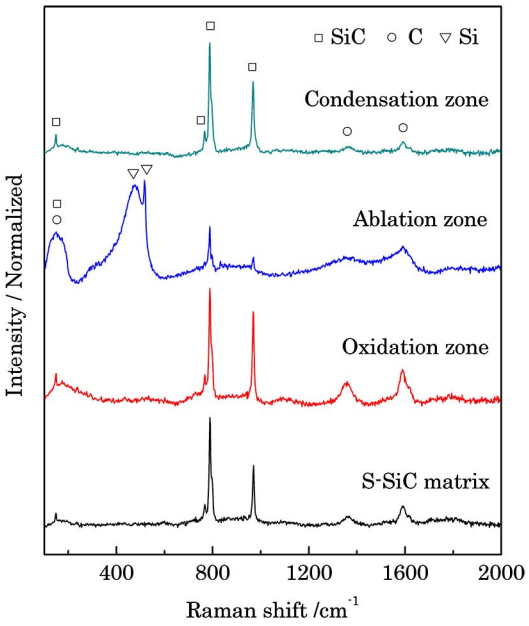

Fig. 4. Phases of the SiC zones at 3.1 J/cm^2, 50 pulses.

are the same as the SiC matrix, and no distinguishable Si-O bond peak is found. Since the O exists in many forms, the existence form of the O element needs further study.

The ablation characteristics are similar at laser fluences of 1.0, 2.1, and 3.1 J/cm^2, so we believe the above analysis should be typical. The excimer laser ablation process of the S-SiC ceramics could be made clear. When the laser is ablated, the material absorbs the energy and heats up sharply. Studies on thermal reaction of SiC found that it could decompose before incomplete melting and form an equilibrium liquid phase with Si and C at 2830–3160°C[20,21]. The photochemical effect of the laser may intensify the decomposition further. When this liquid phase cools down below the decomposition temperature, Si tends to react with the decomposed and free C to generate the SiC phase. But the liquid solidifies before large amounts of Si-C, Si-O, and C-O bonds combine, so the final phases of the ablation zone are mainly Si and C phase. The material of the affected zone has not reached its decomposition, melting, and vaporization temperatures, but the heat significantly increases the reaction rate of SiC with the O element. So the C element reduces by forming gaseous C-O products, and oxygen-containing products are retained.

Although no essential differences are found in the phase and melting rules, laser parameters affect the ablation degree of SiC. Figure 5 shows the melting and oxidation degree of SiC, which increases with the laser fluence from 1.0 to 4.0 J/cm^2. F_{th} is determined by the morphology observation method as 0.4 J/cm^2, so the laser fluence from 0.5 to 4 J/cm^2 with different pulses is chosen to study the ablation.

Figure 6(a) shows the ablation depth of SiC ceramics with different laser fluence and pulses. When the pulse number or the fluence is low, stable depth data is difficult

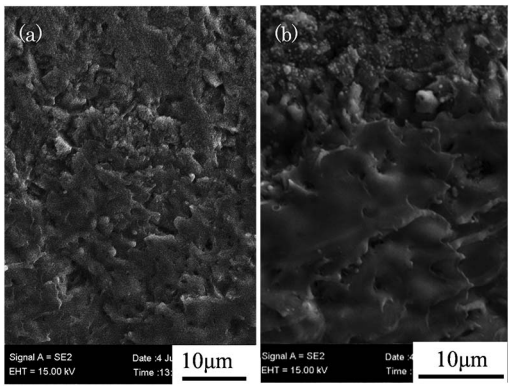

Fig. 5. Morphology of the SiC with laser fluence of (a) 1.5 J/cm^2 and (b) 4 J/cm^2, 10 pulses.

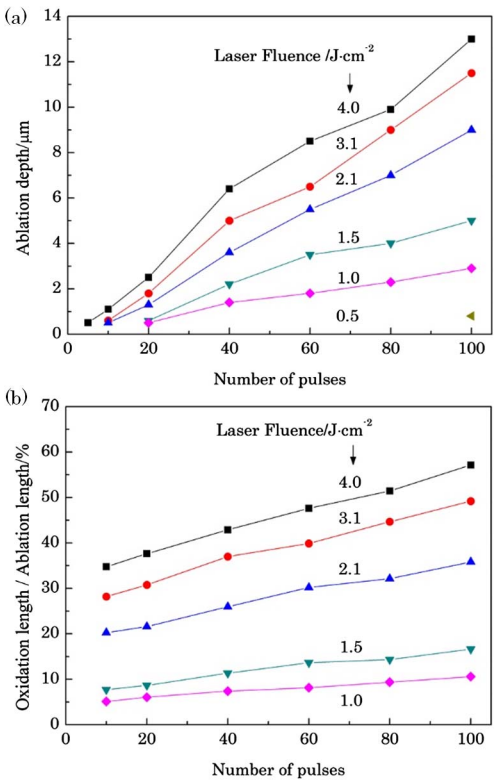

Fig. 6. (a) Ablation depth and (b) oxidation length.

to obtain, so they are not counted. The ablation depth increases almost linearly with pulses and laser fluence, respectively, the ablation rate is 0.13 μm/pulse at 4 J/cm^2 and 0.03 μm/pulse at 1 J/cm^2. So, in the range of 0.5 to 4 J/cm^2, plasma shielding phenomenon does not occur and the ablation is based on the continuous absorption of pulse energy. The constant ablation rate reveals that the ablation effect of SiC by the excimer laser is mainly removal and the melting is limited.

The laser parameters could influence the range of the oxidation zone. Figure 6(b) shows the ratio of oxidation length/ablation length, where the oxidation length is the distance from the condensation zone to the matrix. The oxidation length is increasing linearly with the laser fluence and pulses, which is consistent with the regulation of ablation depth. The 10 ns pulse width of the excimer laser could account for this. It is far greater than the coupling time between the electron and the crystal lattice, so the impulse energy is redistributed mainly in the form of heat transfer. The laser fluence and pulses both increase the total energy absorbed by the SiC ceramics, leading to the expansion of the oxidation zone. In addition, the energy is not uniformly distributed in the whole spot, and the marginal density is slightly lower. The increase in laser fluence could directly make the marginal density exceed F_{th}, but the addition of pulse numbers could not. So the ablation length increases slightly with the fluence, but stays the same with different pulses.

The ablation efficiency of the S-SiC ceramics can be characterized by the ratio of ablation rate/the corresponding laser fluence[22], as shown in Fig. 7. In the range of 0.5–4 J/cm^2, the laser ablation efficiency is 3.60 ± 0.60 μm · mm^2/J. The ablation effect is not dependent on the energy density, and the single-photon ablation effect is consistent. Therefore, the primary action unit of the dominant mechanism of the excimer laser ablation of S-SiC ceramics is single-photon absorption. According to the SSB (Srinivasan–Smrtic–Babu) theory, the total ablation of the material irradiated by the UV laser includes photochemical ablation and photothermal ablation[23]. The single photon of the 193 nm laser can break the Si-C chemical bond, and the energy redistribution is achieved by heat transfer, so both effects are realized by single-photon absorption.

However, since photochemical ablation is realized by single-photon absorption, according to Beer–Lambert's law, the photochemical ablation depth (D_{pc}) can be expressed as

$$D_{\text{pc}} = \frac{1}{\alpha} \ln \frac{F}{F_{\text{th}}}, \tag{1}$$

where F is the laser fluence, F_{th} is the ablation threshold of the material, and α is the absorption coefficient of the material. For α-SiC, the main phase of the S-SiC, α is 1.1×10^6 cm^{-1} at 193 nm.

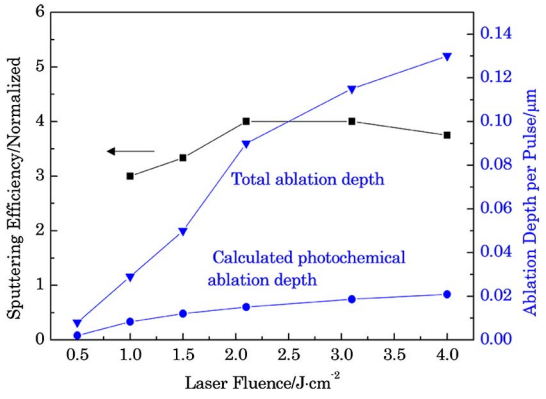

Fig. 7. Ablation efficiency and ablation depth.

Figure 7 also shows the comparison of the total ablation depth (D_t) and calculated D_{pc}. The D_{pc} increases with the laser fluence, and it accounts for about 25% of D_t at 1 J/cm^2, but the proportion has reduced to 16% at 4 J/cm^2. The photothermal effect increases with the laser fluence. Combined with the melting morphology of the ablation zone and the thermal oxidation characteristics of the affected zone, the 193 nm laser ablation of S-SiC ceramics is mainly dominated by the photothermal effect and conforms to the thermal evaporation mechanism. Although the laser has a large photon energy, the 20 ns pulse width, which is much longer than the coupling time between the electron and the lattice, allows the energy to be redistributed through the heat transfer, greatly limiting the "cold effects". The heat could cause a small amount of melting on the SiC surface, effectively repairing the original pores and scratches on the ceramic. As shown in Fig. 2, the porosity and scratch rate of the ceramic irritated by the excimer laser [Fig. 2(b)] decreased by 86% compared to the original one [Fig. 2(a)], and little oxidation of the ablation zone was caused. Since the surface defects are the main crack sources of ceramic materials, the repair effect of this photothermal reaction is beneficial to the performance, life, and reliability of ceramic materials. However, since the morphology variation and ablation depth under low fluence and low pulses are indistinguishable in this experiment, the ablation effect near the ablation threshold and under low pulses is not discussed. To comprehensively understand the ablation mechanism, further studies are needed.

In conclusion, the ablation effects and mechanism of S-SiC ceramics by a 193 nm ArF excimer laser were studied, under the premise of reducing the environmental impact. The SiC generates three zones: the ablation zone, which presents molten morphology and is composed by Si phase and graphite or amorphous carbon; the condensation zone, which is formed by vaporized SiC; and the oxidation zone, which has the characteristics of thermal oxidation. The ablation depth and oxidation range increase linearly with fluence and pulses within 0.5–4 J/cm^2, but the normalized ablation efficiency is stable ($3.60 \pm 0.60\,\mu m \cdot mm^2/J$). The theoretical photochemical ablation depth supplies 25% of the total depth at 1 J/cm^2 but decreases to 16% at 4 J/cm^2. So the single-photon ablation effect is identical and the thermal effect increases with fluence. The ablation of S-SiC ceramics is dominated by the photothermal effect and mainly conforms to the thermal evaporation mechanism.

This work was supported by the National Natural Science Foundation of China (No. 61705235) and the Innovation Project of the Academy of Opto-Electronics, Chinese Academy of Sciences (No. Y70B03A12Y).

References

1. Z. U. Rehman and K. A. Janulewicz, Appl. Surf. Sci. **385**, 1 (2016).
2. Y. Cheng, X. Huang, Z. Du, and J. Xiao, Opt. Mater. **73**, 723 (2017).
3. Q. Gong, J. Shen, and J. Xie, J. Synth. Cryst. **7**, 1898 (2016).
4. J. Q. Wang, X. L. Tian, B. G. Zhang, and P. X. Wang, China Surf. Eng. **3**, 81 (2013).
5. A. N. Samant and N. B. Dahotre, J. Eur. Ceram. Soc. **29**, 969 (2009).
6. J. Meijer, K. Du, A. Gillner, D. Hoffmann, V. S. Kovalenko, T. Masuzawa, A. Ostendorf, R. Poprawe, and W. Schulz, CIRP Ann. **51**, 531 (2002).
7. C. G. Moura, R. S. F. Pereira, M. Andritschky, A. L. B. Lopes, J. P. D. F. Grilo, R. M. D. Nascimento, and F. S. Silva, Opt. Laser Technol. **97**, 20 (2017).
8. M. Cai, X. Zhang, W. Zhang, L. Ji, J. Jiao, and H. P. Qiu, Aeronaut. Manuf. Technol. **19**, 52 (2016).
9. M. S. Amer, M. A. El-Ashry, L. R. Dosser, K. E. Hix, J. F. Maguire, and B. Irwin, Appl. Surf. Sci. **242**, 162 (2005).
10. X. Li, "*Study on the surface roughness control model of SiC in femtosecond laser processing*," Tianjin Polytechnic University, 72 (2016).
11. P. Baeri, C. Spinella, and R. Reitano, Int. J. Thermophys. **20**, 1211 (1999).
12. D. Sciti, C. Melandri, and A. Bellosi, J. Mater. Sci. **35**, 3799 (2000).
13. X. Hua, X. Wei, M. Zhou, and X. Xie, Chin. J. Lasers. **41**, 1203002 (2014).
14. X. Xie, X. Huang, W. Chen, X. Wei, W. Hu, and R. Che, Chin. J. Lasers **40**, 1203010 (2013).
15. L. Li, "*The research of 248 nm excimer laser interaction with three kinds of inorganic nonmetal optical materials*," Wuhan University of Technology, 72 (2014).
16. D. H. Duc, I. Naoki, and F. Kazuyoshi, Int. J. Heat Mass Transfer **65**, 713 (2013).
17. C. Dutto, E. Fogarassy, and D. Mathiot, Appl. Surf. Sci. **184**, 362 (2001).
18. R. Zhang, "*Machining technology and properties investigation of SiC/SiC composites by ultra-short pulse laser,*" Xi'an Institute of Optics and Precision Mechanics, Chinese Academy of Sciences, 89 (2016).
19. S.-K. Shin, C. Huang, and F.-S. Yu, Acta. Phys. Sin. **20**, 654 (1964).
20. K. Daviau and K. K. M. Lee, Phys. Rev. B **96**, 174102 (2017).
21. D. Amans, M. Diouf, J. Lam, G. Ledoux, and C. Dujardin, J. Colloid Interface Sci. **489**, 114 (2017).
22. A. J. Pedraza, Nucl. Instrum. Meth. B **141**, 709 (1998).
23. S. V. Babu and G. C. D. D. Egitto, J. Appl. Phys. **72**, 692 (1992).